Journal of Power Sources 196 (2011) 9087–9095

Contents lists available at ScienceDirect

Journal of Power Sources

journal homepage: www.elsevier.com/locate/jpowsour

Hydrogen production by reforming of diesel fuel over catalysts derived from $LaCo_{1-x}Ru_xO_3$ perovskites: Effect of the partial substitution of Co by Ru ($x = 0.01–0.1$)

N. Mota [a,*], R.M. Navarro [a,*], M.C. Alvarez-Galvan [a], S.M. Al-Zahrani [b], J.L.G. Fierro [a]

[a] Instituto de Catálisis y Petroleoquímica (CSIC), Marie Curie 2, Cantoblanco 28049, Madrid, Spain
[b] Chem. Eng. Dpt., College of Engineering, King Saud University, Saudi Arabia

ARTICLE INFO

Article history:
Received 29 October 2010
Received in revised form
22 November 2010
Accepted 25 November 2010
Available online 2 December 2010

Keywords:
Hydrogen
Diesel
Perovskite
Cobalt
Lanthanum
Ruthenium

ABSTRACT

$LaCo_{1-x}Ru_xO_3$ perovskites with different substitutions of Co by Ru ($x = 0.01–0.1$) have been investigated as precursors of catalysts for the oxidative reforming of diesel for hydrogen production. The physicochemical characterization of $LaCo_{1-x}Ru_xO_3$ perovskites revealed modifications in their structure, crystalline size and surface area with the incorporation of ruthenium into the perovskite lattice. The modifications in the perovskites affect the structure and morphology of the catalysts obtained by reduction of perovskites prior the reaction. In the catalysts derived from ruthenium-containing perovskites it is observed a better reducibility, smaller particle size of La_2O_3 and Co^0 phases and better surface concentration of Ru^0 particles with the increase in the degree of Co substitution in the perovskite. The modifications in the characteristics of the catalysts induced by the Co substitution in perovskite directly affect their catalytic behaviour in the oxidative reforming of diesel. It is found that the greater $Co^0 + Ru^0$ exposition and the higher extension of the $La_2O_2CO_3$ phase achieved in catalysts derived from perovskites with higher cobalt degree of substitution produces an increase in the activity and stability of the catalysts derived.

1. Introduction

Hydrogen production is a key target in the development of future alternative energy systems for providing a clean and affordable energy supply [1–6]. Nowadays, there is an increasing interest in the development of technologies for the conversion of liquid hydrocarbons in hydrogen rich gas mixtures as a way to overcome the current technical limitations in hydrogen supply and storage. In spite of the doubts about the viability of hydrocarbons derived from crude oil from the point of view of overall system efficiency and renewability, this option entails no extra capital cost for developing infrastructure and this might contribute to reducing the cost of introducing hydrogen in energy systems [5–9]. A further advantage is that developments in the field of hydrogen generation from conventional fuels could be applied to the extraction of hydrogen from other liquid fuels containing heavy hydrocarbons produced from biomass, thereby providing a bridge for the transition in hydrogen production from fossil fuels to renewable production from biomass. Among the liquids fuels that can be reformed, diesel is an interesting option owing to its low price, wide distribution infrastructure, ease of handling and high-energy density.

The catalytic hydrocarbon reforming process is currently the best developed and most economical technique for H_2 production from liquid fuels. Among the conventional reforming processes, the oxidative steam reforming (OSR) [3] offers advantages over the individual steam reforming (SR) and catalytic partial oxidation (CPOX) in terms of efficiency and dynamic response allowing smaller reactor volume and simpler design [10–12].

Conventional catalysts formulations developed for diesel reforming process typically consist in noble metals (Pt, Rh) or non noble metals (Ni, Co) [13–15] incorporated into carefully designed supports such as thermally stabilized doped alumina, mixed metal oxides or oxide-ion-conducting substrates like ceria, zirconia or lanthanum gallate doped with gadolinium or samarium [16–19]. An alternative to conventional catalysts are perovskites (ABO_3) that have been studied as catalysts or catalyst precursors due to the possibility of obtaining well-dispersed and stable active metal particles (B^0) under reforming conditions. Catalysts derived from lanthanum cobaltite perovskite ($LaCoO_3$) have been reported as being very efficient for the production of hydrogen by oxidative reforming of heavy hydrocarbons [20–22]. The Co^0/La_2O_3 catalysts derived from $LaCoO_3$ perovskite have recorded very high hydrogen yields and high stability for the oxidative reforming of real diesel

* Corresponding authors. Tel.: +34 915854773; fax: +34 915854760.
E-mail addresses: noelia.mota@icp.csic.es (N. Mota), r.navarro@icp.csic.es (R.M. Navarro).

0378-7753/$ – see front matter © 2010 Elsevier B.V. All rights reserved.
doi:10.1016/j.jpowsour.2010.11.143

Table 1
Nominal composition and tolerance factor of $LaCo_{1-x}Ru_x$ perovskites (catalyst precursors).

	Atomic composition La/Co/Ru	Tolerance factor (t)
LaCo	1/1/0	0.971
$LaCoRu_{0.01}$	1/0.99/0.01	0.971
$LaCoRu_{0.05}$	1/0.95/0.05	0.969
$LaCoRu_{0.1}$	1/0.90/0.10	0.968

fuel containing 12 ppmw of sulphur [20]. A strategy to improve the activity and stability of Co^0/La_2O_3 catalysts derived from $LaCoO_3$ is introducing structural modifications in the perovskite by means of the partial substitution of cobalt by other transition metals (Ni, Ru, Fe, Cr, Mn, etc.) [23–26]. Among the transition metals that can be introduced in the structure of $LaCoO_3$, ruthenium is of particular interest because it is highly effective in the catalytic reforming of heavy hydrocarbons [20,21].

With this background, the objective of this work was to study the influence of the partial substitution of Co by Ru over the physicochemical properties of $LaCo_{1-x}Ru_xO_3$ (x = 0.01–0.1) perovskites and its influence on the structure and activity of the catalysts derived from them to produce hydrogen by oxidative reforming of diesel. Surface and structural characteristics of perovskites have been analyzed, trying to establish a relationship between the physicochemical characteristics of perovskites and the structure, activity and stability of the catalysts derived from them.

2. Experimental

2.1. Perovskites preparation

Perovskites were synthesized by a modified citrate sol–gel method [27]. 1 M aqueous solutions of $La(NO_3)_3{\cdot}6H_2O$ (99.9% Alfa Aesar), $Co(NO_3)_2{\cdot}6H_2O$ (97.7% Alfa Aesar) and $RuCl_3$ (40.49% Ru, Johnson Matthey) were added to a solution of citric acid (Alfa Aesar) and ethylene glycol (Riedel-de Haën) in adequate amounts (citric acid/(A-cation + B-cation) = 2.5 mol and ethylene glycol/citric acid = 1 mol). The aqueous mixture was stirred and slowly heated to 343 K. The resultant solution was dried at 363 K for 2 h obtaining a resin which contains the metal cations inside a polymeric network. After that, the resin was milled to obtain a fine powder that was dried at 573 K for 2 h and calcined under air at 1023 K for 4 h with a heating rate of 2 K min^{-1}. Table 1 shows the nominal chemical composition, expressed as relative atomic composition, of the perovskites prepared in this work as catalyst precursors.

2.2. Physicochemical characterization

The BET surface area of the perovskites was calculated by adsorption/desorption of nitrogen at 77 K, taking a value of 0.162 nm^2 for the cross-section of N_2 molecule adsorbed at this temperature. These measurements were performed with a Micromeritics ASAP 2100 apparatus on samples previously degassed at 423 K for 12 h. The experiments were performed at liquid nitrogen temperature (77 K) using quasi-Gemini method to minimize errors in the measurement of low area samples.

XRD patterns of perovskites and catalysts derived from them were recorded using a Seifert 3000P vertical diffractometer and nickel-filtered Cu Kα radiation (λ = 0.1538 nm) under constant instrumental parameters. For each sample, Bragg angles between 5° and 100° were scanned; a rate of 5 s per step (step size: 0.04° 2θ) was used during a continuous scan in the above-mentioned range. The mean crystalline particle size was estimated from X-ray line width broadening using the Scherrer equation. Width (t) was taken through the full width at half maximum intensity of the most intense and least overlapped peaks.

XPS measurements were recorded using an Escalab 200R spectrometer equipped with a hemispherical electron analyser and an Al Kα ($h\nu$ = 1486.6 eV, 1 eV = 1.6302×10^{-19} J) 120 W X-ray source. The area of the peaks was estimated by calculating the integral of each peak after smoothing and subtraction of an S-shaped background and fitting of the experimental curve to a mixture of Lorentzian and Gaussian lines of variable proportions. All binding energies (BE) were referenced to the C 1s signal at 284.6 eV from carbon contamination of the samples to correct the charging effects. Quantification of the atomic fractions on the sample surface was obtained by integration of the peaks with appropriate corrections for sensitivity factors [28].

Hydrogen temperature-programmed reductions (H_2-TPR) of the perovskites were conducted using a PID Eng & Tech instrument in a U-shaped quartz reactor. Prior to the reduction experiments, the sample (15 mg) was flushed with a helium stream at 383 K for 15 min and then cooled down to room temperature. TPR profiles were obtained by heating the sample under a 10% H_2/Ar flow (50 mL min^{-1}) from 303 to 973 K (1 h at 973 K) at a linearly programmed rate of 10 K min^{-1}.

2.3. Activity tests

Diesel reforming tests were performed using 100 mg of catalyst in a fixed-bed continuous-flow stainless steel reactor (8-mm i.d.) with a coaxially centred thermocouple in contact with the catalytic bed. Before the catalytic tests, the perovskites were transformed into active catalysts by reduction under a 10% H_2/N_2 flow using the conditions derived from TPR profiles (50 mL_N min^{-1}, T = 973 K for 1 h).

The flow rates of the diesel and water feeds were controlled by liquid pumps and the feed were preheated in an evaporator at 473 K before being passed through the catalyst bed in the reactor. Diesel fuel was provided by CEPSA (R&D Center) and its sulphur amount was 22 ppmw. For the oxidative reforming of diesel, the reactants were introduced into the reactor at a molar ratio of $H_2O/O_2/C$ = 3/0.5/1. The total gas flow rate was kept at 75 mL min^{-1} (GHSV = 20,000 h^{-1}) and the reaction temperature was 1023 K to avoid maximum conversion. Activity was measured for 24 h and the reaction products were analyzed periodically with an on-line gas chromatograph (Varian 450-GC) equipped with a TC detector which was programmed to operate under high-sensitivity conditions.

The diesel conversion and selectivity of products are defined as follows:

- Diesel conversion (%):

$$\frac{(\text{mole } C_mH_n)_{in} - (\text{mole } C_mH_n)_{out}}{(\text{mole } C_mH_n)_{in}} \times 100 \quad (1)$$

- Selectivity (%) (i: H_2, CO, CH_4, CO_2, C_2H_4, $C_2H_6$and C_3H_6):

$$\frac{(\text{mole } i)_{out}}{(\text{mole } C_mH_n)_{in} - (\text{mole } C_mH_n)_{out}} \times 100 \quad (2)$$

3. Results

3.1. Characterization of perovskites (catalyst precursors)

3.1.1. Surface area and X-ray diffraction (XRD)

All the perovskites presented isotherms of type H3 (not shown) characteristic of macroporous solids with a weak interaction with the adsorbate. Textural data obtained from N_2 adsorption–desorption isotherms indicate that the surface area of the perovskites (Table 2) displayed low values of both surface area

Table 2
BET specific surface area and mean crystalline particle size from XRD of $LaCo_{1-x}Ru_x$ perovskites (catalyst precursors).

	BET specific surface area ($m^2\ g^{-1}$)	XRD particle size of $LaCo_{1-x}Ru_xO_3$ (x = 0–0.1) (nm)
LaCo	1.1	54
$LaCoRu_{0.01}$	2.6	51
$LaCoRu_{0.05}$	3.1	24
$LaCoRu_{0.1}$	5.8	16

and pore volume supporting that perovskites do not develop a nanoporous structure. In spite of that, it is observed an increase in the surface area of the perovskites with the increase in the partial substitution of Co by Ru in the perovskite. Taking into account that specific surface areas exposed by perovskite crystals are equal to the geometrical one, as they do not possess internal microporosity, the observed changes in surface area with the incorporation of Ru could be indicative of structural changes and/or crystal growth of perovskite induced by the insertion of Ru.

X-ray diffraction patterns of perovskites are showed in Fig. 1. All patterns presented strong reflexions corresponding to the presence of a well-defined perovskite structure with high degree of crystallinity and homogeneity. The XRD patterns of the calcined LaCo and $LaCoRu_{0.01}$ samples exhibit the strong doublet reflections close to 32.9° (1 1 0) and 33.3° (1 0 4) that correspond to the stoichiometric perovskite with rhombohedric deformation of the ideal cubic structure of perovskite (JCPDS 48-123). The diffraction pattern of the calcined $LaCoRu_{0.05}$ and $LaCoRu_{0.1}$ samples show an ill-resolved doublet reflection shifted to lower 2θ-angle values indicative of a rhombohedral structure with cell parameter modified (JCPDS 86-1662). As observed in Fig. 1, the partial substitution of cobalt by ruthenium in perovskites leads to single perovskite structures without peaks attributable to ruthenium oxides. This fact is indicative of a high degree of incorporation of the Ru into the perovskite structure. In line with this, the diffraction lines of the Ru-substituted perovskites shifted to lower angles respect to the diffraction lines characteristic of rhombohedral $LaCoO_3$ perovskite phase (JCPDS 48-123) that results in a modification of the rhombohedral structure in LaCo sample to an orthorhombic structure in the $LaCoRu_{0.1}$ sample. Taking into account the differences in the ionic radii of Co^{3+} (0.61 Å) and Ru^{3+} ions (0.68 Å), the observed

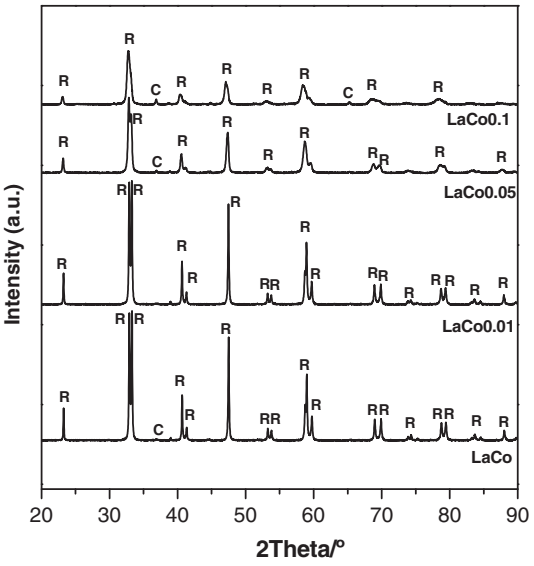

Fig. 1. XRD patterns of $LaCo_{1-x}Ru_xO_3$ perovskites (precursors of catalysts) (R: $LaCoO_3$ rhombohedraland C: Co_3O_4 cubic).

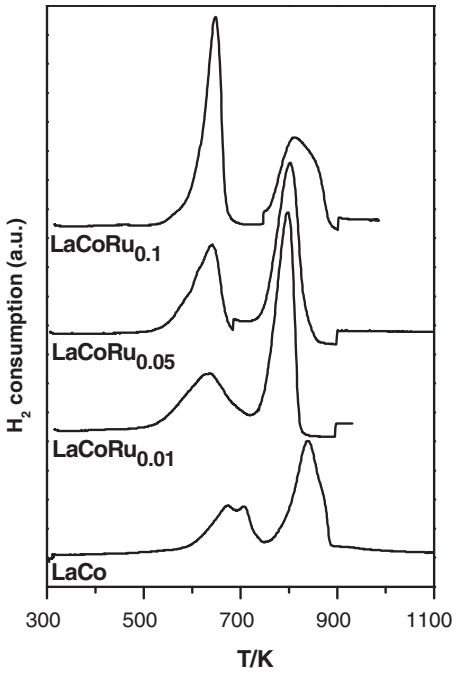

Fig. 2. TPR profiles of $LaCo_{1-x}Ru_xO_3$ perovskites (precursors of catalysts).

modifications of the XRD patterns indicated an increase in the insertion degree of Ru ions into the $LaCoO_3$ lattice [29]. The ideal perovskite structure has a cubic unit cell. Nevertheless, distortions are common and depend on the value of the tolerance factor t, a geometrical quantity defined as $r_A + r_O/\sqrt{2}(r_B + r_O)$ (r_A, r_B, r_O = A, B and oxygen ion radius). As tolerance factor decreases from 1, the perovskite structure deforms towards structures with lower coordination for A. In the case of $LaCoO_3$ perovskite, a rhombohedral distortion usually results while for lower values, as in the case of $LaRuO_3$ perovskite, orthorhombic structures were observed [30]. Therefore, when the Co^{3+} are replaced partially by higher Ru^{3+} ions it leads to an increase of the average B site ion radius and a decrease of tolerance factor t (Table 1) that is in line with the deformation of the rhombohedral lattice observed with the increase in the partial substitution of Co by Ru ions in the perovskite.

Quantitative evaluation of crystallite sizes of $LaCo_{1-x}Ru_xO_3$ (x = 0–0.1) perovskites, calculated by applying the Scherrer equation has also been calculated (Table 2). It can be noted that mean crystallite size of the perovskites was affected by the degree of Ru substitution in the perovskite. It is observed a decrease in the crystalline size of perovskites with the increase in the degree of substitution of Co in the $LaCoO_3$ structure. The lower particle size of the perovskite phase when Co is substituted by Ru derived from the higher line broadening of the XRD diffraction peaks of perovskite (Fig. 1) is indicative of a lower growth capacity of the perovskite crystal domains when Ru is present in the perovskite structure.

3.1.2. Temperature programmed reduction (TPR)

TPR profiles of the prepared perovskites are depicted in Fig. 2. The reduction profile of LaCo sample reveals two hydrogen consumption peaks at temperatures around 700 K and 838 K, which indicate the reduction of the perovskite in two consecutive steps. An additional reduction peak at low temperature was observed at 673 K. This additional peak is related to the reduction of cobalt oxide species not incorporated into the perovskite structure. Several studies in the literature have proposed an explanation for the two steps of reduction of the Co^{3+} in $LaCoO_3$ [20]. According to this explanation, the low-temperature peak is associated to the first

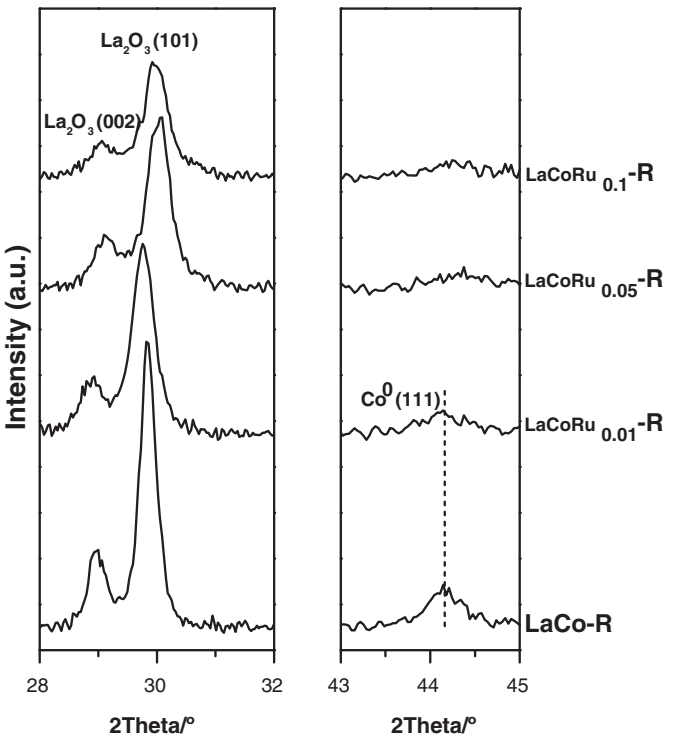

Fig. 3. XRD patterns of catalysts obtained after thermal reduction of $LaCo_{1-x}Ru_xO_3$ perovskites.

reduction step of Co^{3+} to Co^{2+} in the perovskite structure forming Brownmillerite-type oxides ($2LaCoO_3 + H_2 \rightarrow 2LaCoO_{2.5} + H_2O$) while the second and more intense reduction peak is assigned to the reduction of Co^{2+} to highly dispersed Co^0 over La_2O_3.

Ru-substituted perovskites also reveal a two step reduction with hydrogen consumption peaks at temperatures around 640 K and 800 K. The low-temperature peak include the reduction of Ru^{3+} and Co^{3+} ions in perovskite to Ru^0 and Co^{2+} respectively together with the reduction of some cobalt oxide phases not incorporated into the perovskite structure. As in the case of the LaCo sample, the reduction peak at high temperature was attributed to the subsequent reduction of Co^{2+} ions to Co^0 and La_2O_3. It is observed a marked effect of the Ru substitution in the reduction behaviour of the perovskites. The peaks corresponding to the two steps reduction of perovskite shift to lower temperature with the substitution of Co by Ru. The shift of the reduction peaks to lower temperatures with the incorporation of ruthenium may be due to a spill-over process of hydrogen assisted by the formation of metallic ruthenium in the first reduction step [31,32], or related to modifications in the perovskite structure or size that lead to structures with lower diffusional resistance of hydrogen from the external surface of the particles through the inner, favouring the whole reduction process [20,33,34]. In line with this latter explanation, the difference in reduction temperature may be associated to the deformation of the rhombohedral lattice and lower size of the perovskite structure observed with the increase in the degree of substitution of Co in the $LaCoO_3$ structure.

3.2. Characterization of catalysts

3.2.1. X-ray diffraction (XRD)

Perovskites are transformed in catalysts after reduction under hydrogen at 973 K (see Section 2.3). The XRD patterns of the catalysts obtained by reduction of perovskites are shown in Fig. 3. The reduction of perovskites produces a complete transformation of the perovskite structure which decomposes into a Co^0 phase with a cubic structure (JCPDS 1-1259), with diffraction lines at 44.4° (1 1 1), and La_2O_3 (JCPDS 5-602), with reflections at 29.1° (0 0 2) and 30.0° (1 0 1). None of the catalysts show diffraction peaks corresponding to crystalline forms of metallic ruthenium phases at $2\theta = 44.1°$ (JCPDS 65-7645). The presence of these crystalline phases is consistent with the mechanism of reduction of $LaCoO_3$ perovskite described in the previous TPR section. However as observed in Fig. 3, the characteristics of crystalline phases of Co and La_2O_3 after reduction of perovskites depending on the degree in the partial substitution of Co by Ru. It is observed a decrease in the intensity of the diffraction lines corresponding to crystalline phases of La_2O_3 and Co^0 with the rise in the substitution of Co in the perovskites used as catalyst precursors. Moreover, for $LaCoRu_{0.05}$ and $LaCoRu_{0.1}$ catalysts it is also observed a shift in the reflections of the La_2O_3 crystalline phases, which indicate changes in the cell parameters of the La_2O_3 structures associated with the presence of ruthenium.

Quantitative estimation of the average particle size of La_2O_3 and Co^0 in the catalysts, calculated by applying Scherrer equation, is displayed in Table 3. It can be observed a decrease in the particle size of La_2O_3 crystallites formed after reduction of the perovskites containing ruthenium. Similarly, it has been also found a decrease in the crystalline domains of Co^0 formed after reduction of perovskites with higher degree of cobalt substitution by ruthenium.

Table 3
Mean crystallite size of La_2O_3 and Co^0 in catalysts obtained after thermal reduction of $LaCo_{1-x}Ru_xO_3$ perovskites.

	La_2O_3 (nm)	Co^0 (nm)
LaCo–R	23	20
$LaCoRu_{0.01}$–R	18	14
$LaCoRu_{0.05}$–R	18	n.d.
$LaCoRu_{0.1}$–R	16	n.d.

n.d.: not detected.

3.2.2. X-ray photoelectron spectroscopy (XPS)

Photoelectron spectroscopy analyses were performed in order to determine the chemical state of the elements and their surface proportions on catalysts. The La 3d core level of pure La_2O_3 exhibits (Fig. 4) a main component of the $La3d_{5/2}$ core level at binding energies of 834.7–835.1 eV. The LaCo catalyst exhibit a significant broadening of the La 3d core level (Fig. 4) indicative of a second contribution at 834.1 eV attributed to the presence of La^{3+} in perovskite and/or $La(OH)_3$ structures [26,35,36]. The La 3d doublets in Ru-substituted catalysts (Fig. 4) are more resolved and similar to that observed in the spectrum of pure La_2O_3. This fact points to surface changes in La structures after the reduction induced by the presence of ruthenium in the perovskites used as precursors that facilitates the presence of surface La as La_2O_3.

The Co 2p core level of all catalysts (Fig. 5) shows a shape and binding energies values (779–780 eV) characteristic of the coexistence of cobalt species in the form of perovskite and in the form of metallic phase on the surface. Furthermore, the Co 2p level of LaCo–R and $LaCoRu_{0.05}$–R catalysts shows a shake-up peak at 789 eV and 787 eV, respectively, indicative of the presence of surface oxide phases (Co_3O_4 and/or CoO) [37–40].

In relation to the chemical state of ruthenium species, the Ru $3p_{3/2}$ level of catalysts (Fig. 6) showed a main component at 462.2 eV characteristic of the presence of metallic species of ruthenium on the surface of all catalysts [20].

The surface concentration of La, Co and Ru on catalysts calculated from XPS intensities is presented in Fig. 7. For the samples containing Ru, it is observed a decrease in the lanthanum surface concentration respect to the sample derived from $LaCoO_3$ perovskite. However, the surface concentration of lanthanum in

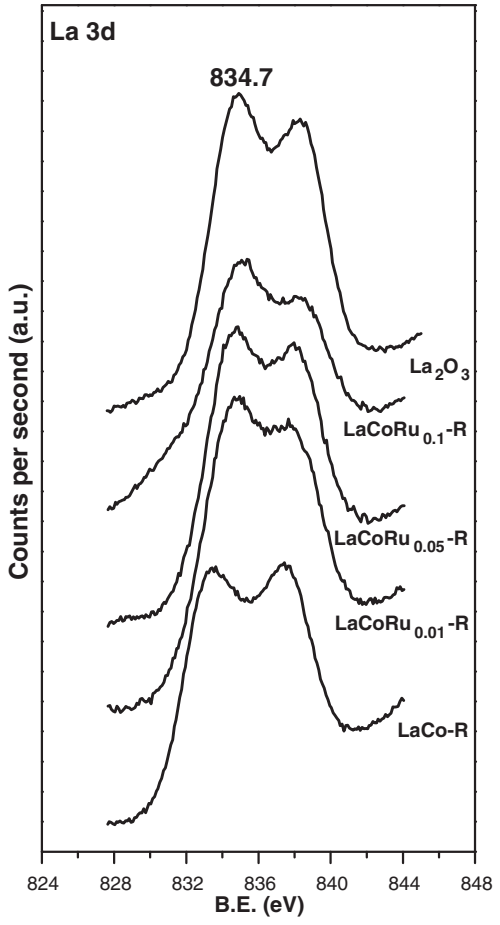

Fig. 4. La3d$_{5/2}$ XPS spectra of catalysts obtained after thermal reduction of$LaCo_{1-x}Ru_xO_3$ perovskites.

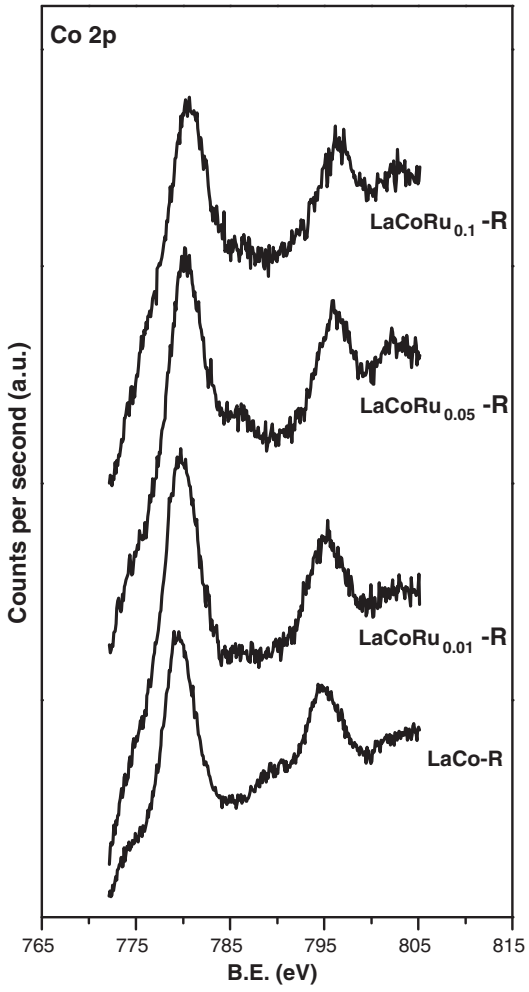

Fig. 5. Co 2p XPS spectra of catalysts obtained after thermal reduction of$LaCo_{1-x}Ru_xO_3$ perovskites.

catalysts containing Ru was not significantly modified with the partial substitution degree of cobalt by ruthenium. In all catalysts, the Co surface concentration is lower than nominal, indicating a pronounced loss of cobalt at surface level. The cobalt surface concentration was similar in all catalysts irrespective of the degree of partial substitution of cobalt by ruthenium in the perovskites used as catalyst precursors. In all catalysts, the ruthenium surface concentration was higher than nominal and dependent on the Ru substitution degree in the perovskite. As it is shown in Fig. 7, the surface concentration of ruthenium in catalysts varies according the sequence: $LaCoRu_{0.1}$–R > $LaCoRu_{0.05}$–R ≈ $LaCoRu_{0.01}$–R.

3.3. Catalytic activity tests

The activity of the catalysts derived from LaCo, $LaCoRu_{0.01}$, $LaCoRu_{0.05}$ and $LaCoRu_{0.1}$ perovskites was evaluated in the oxidative reforming of diesel performed, as indicated in the experimental section, at atmospheric pressure and 1123 K. Fig. 8 presents the diesel conversion and product distribution for each catalysts as a function of reaction time. It is observed that diesel conversion over catalysts varies with reaction time which is indicative of an evolution of the catalysts under reaction conditions. However, the evolution of the catalysts with reaction time depended on the nature of the perovskite used as catalyst precursor. The catalysts derived from pure $LaCoO_3$ or from perovskites with low degree of Ru substitution ($x < 0.05$) showed lower diesel conversion for short-times on stream (0–4 h) than those obtained for longer times (>4 h). On the contrary, the catalysts derived from the perovskite with higher degree of Ru substitution ($LaCoRu_{0.1}$) does not display an induction period starting with a high diesel conversion but showing a decrease after the first hours on stream. Comparison of diesel conversion values for long times of operation (20–24 h) indicates that all catalysts achieved similar diesel conversion irrespective of the nature of the perovskite used as catalyst precursor.

The evolution of the gaseous products compositions with time on stream (Fig. 8) indicated a different distribution and evolution of the reaction products for each catalyst. The reaction over catalyst derived from bare LaCo perovskite starts with high selectivity to H_2 and carbon oxides but the hydrogen production decreases a 40% throughout the 25 h of reaction. The product evolution with time on stream was also observed on Ru-containing catalysts but to a lesser extent. In contrast with catalysts derived from LaCo perovskite, the initial H_2 selectivity values achieved on Ru-containing catalysts remain more stable with time-on-stream. However the stability of the sites related with the H_2 selectivity appears to be dependent on the Ru content of the catalysts. In this way, it was observed a more stable product composition for catalysts derived from perovskites with higher Ru substitution degree.

3.4. Characterization of used catalysts

3.4.1. X-ray diffraction (XRD)

The diffraction patterns of the used catalysts are displayed in Fig. 9. The used catalysts exhibited diffraction lines at 25.8° (1 0 1), 30.3° (1 0 3), 44.4 (1 1 0) and 47.4° (1 0 7) that correspond to crystalline $La_2O_2CO_3$ phase (JCPDS 37-804) with hexagonal structure.

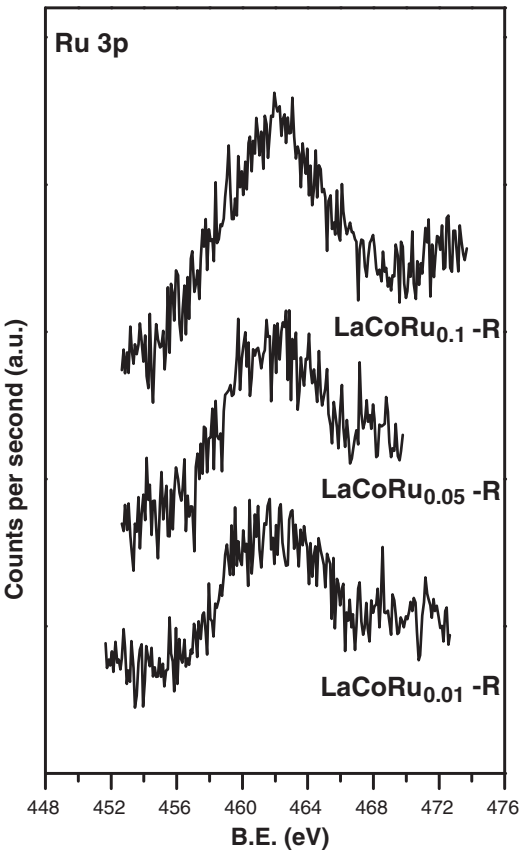

Fig. 6. Ru3p$_{3/2}$ XPS spectra of catalysts obtained after thermal reduction of$LaCo_{1-x}Ru_xO_3$ perovskites.

Table 4
Mean crystalline size of $La_2O_2CO_3$ and intensity ratios of $La_2O_2CO_3$/C from XRD patterns of the used catalysts.

	Particle size$La_2O_2CO_3$ (nm)	$I_{La_2O_2CO_3}/I_C$
LaCo–U	32	10.3
$LaCoRu_{0.01}$–U	33	–
$LaCoRu_{0.05}$–U	30	6.0
$LaCoRu_{0.1}$–U	23	5.6

The XRD patterns of used catalysts also show crystalline phases associated to cubic Co^0 species (JCPDS 15-806), with reflections at 44.2° (1 1 1) and 51.5° (2 0 0) overlapped with diffraction lines corresponding to $La_2O_2CO_3$ phase. Additional reflections at 26.2° (0 0 2) corresponding to graphitic carbon (JCPDS 75-1621) were observed in the LaCo, $LaCoRu_{0.05}$ and $LaCoRu_{0.1}$ used samples.

Quantitative evaluation of the particle size of $La_2O_2CO_3$ in the used catalysts, calculated by applying Scherrer equation, is displayed in Table 4. It can be observed that the average particle diameter of $La_2O_2CO_3$ crystalline phase significantly decreases for $LaCoRu_{0.1}$ used catalyst compared with the rest of the used catalysts. Additionally, Table 4 includes the ratio between the intensities of the reflections at 30.3° and 26.2° corresponding to the $La_2O_2CO_3$ and the graphitic carbon phases, respectively. This sequence reflected the presence of coke with respect to $La_2O_2CO_3$ in the used catalysts decreasing in the order $LaCoRu_{0.01}$ < $LaCoRu_{0.1}$ < $LaCoRu_{0.05}$ < LaCo used catalysts.

4. Discussion

The physicochemical characterization of the $LaCo_{1-x}Ru_xO_3$ perovskites used as precursors of catalysts pointed out that the incorporation of ruthenium provokes significant differences at textural and structural levels. The textural characterization of the perovskites showed a macroporous texture for all samples although with differences in the development of the porous network. The perovskites with Ru exhibited a surface area more developed than that achieved on unsubstituted $LaCoO_3$ counterpart (Table 2). The BET surface area values (Table 2) and the size of the crystalline particles of perovskites calculated by XRD (Table 2) follow opposite trends. This fact agrees with the commonly result in which the surface and the particle size of the perovskites are related since the surface is determined by the geometrical surface of particles without internal porosity. The different introduction degrees of Ru into perovskite structure may be in the origin of the observed changes in particle size. Characterization of perovskites by XRD (Fig. 1) showed a gradual modification in the rhombohedral structure of pure $LaCoO_3$ to orthorhombic structure with the increase in the partial substitution of Co by Ru. Taking into account the differences in the ionic radii of Co and Ru ions, the tolerance factor for perovskite precursors, listed in Table 1, indicates that the incorporation of ruthenium in $LaCoO_3$ structure leads to a decrease in the tolerance factor that is in line with the deformation of the rhombohedral lattice observed with the increase in the partial substitution of Co by Ru ions in the perovskite structure.

The changes in particle size and structure of $LaCo_{1-x}Ru_xO_3$ perovskites with the partial substitution of Co by Ru directly affect its reduction behaviour (Fig. 2) and the structure and morphology of the catalysts formed after the thermal reduction of the perovskites. For all perovskite samples its thermal reduction provokes the complete transformation of the perovskite into the catalysts composed by a mixture of Co^0, Ru^0 and La_2O_3 particles. It is observed a decrease in the crystallite size of La_2O_3 and Co species in parallel to the degree of substitution of Co by in the perovskites (Table 3). These differences in the size of Co^0, Ru^0 and La_2O_3 in catalysts are derived from the initial differences in the particle size and structure of the perovskites induced by the partial substitution of Co by Ru in the $LaCoO_3$ perovskite lattice. In spite of the differences observed in the crystalline size of Co detected by XRD, the Ru-containing catalysts show similar low cobalt surface concentration (Fig. 7). The low Co exposition observed on catalysts after reduction of perovskites may be related with the sintering or volatilization of metallic cobalt particles during the thermal reduction treatment. By contrast, the ruthenium surface exposition on the catalysts after reduction of perovskites was high and their values increase with the substitution of Co by Ru in the perovskites.

As expected, the differences in the physicochemical properties of the catalysts derived from perovskites with different partial substitution degrees of Co by Ru had important implications in their catalytic behaviour in the oxidative reforming of diesel [41]. The comparison of activity measurements with the physicochemical characterization of fresh catalysts point out that the initial activity of the catalysts is directly related with the surface exposition and interaction of the metallic Co and Ru particles with lanthanum oxide particles. Thus, the low initial activity of the catalysts derived from $LaCoO_3$ perovskite (Fig. 8) may be related with its lower surface Co exposition and interaction with La_2O_3 particles (Fig. 7). On the other hand, the higher initial activity of the Ru-containing catalysts is related with the increased metal (Co + Ru) surface exposition observed as the Ru insertion in the perovskite used as catalyst precursor increased (Fig. 7).

For longer times of operation, besides cobalt surface concentration, catalyst deactivation due to the formation of carbon is another factor to be considered in order to describe the evolution of catalysts under reaction. As seen in Fig. 9, lower relative quantities of carbonaceous deposits were observed for Ru-catalysts respect to the catalyst derived from unsubstituted $LaCoO_3$ perovskite in spite of the lower activity of the latter. It is known that both the

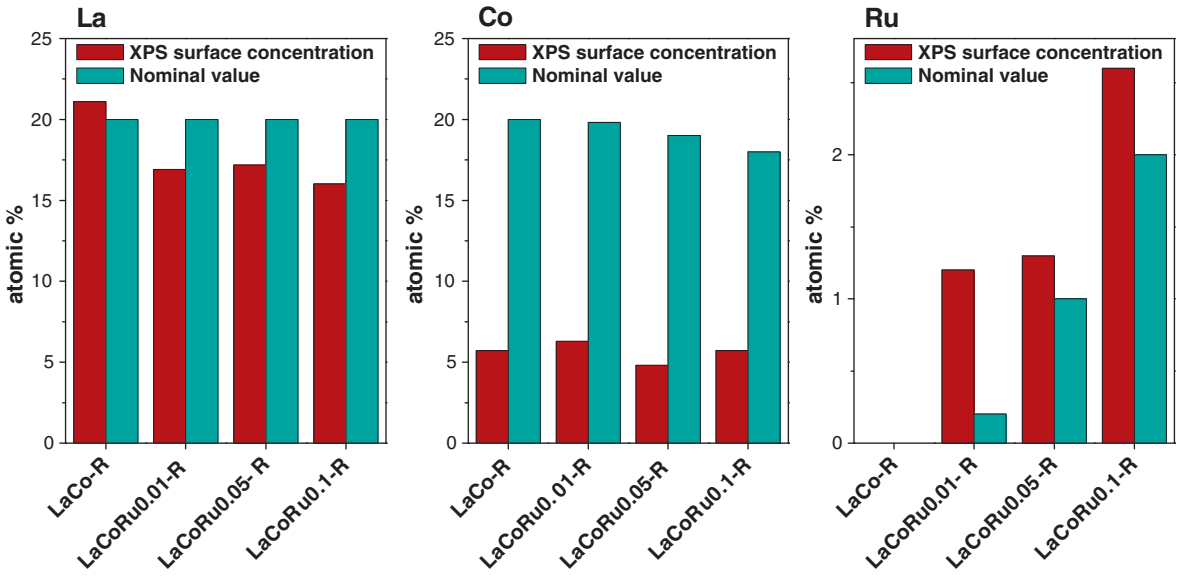

Fig. 7. XPS surface concentration of catalysts (at.%).

active metal particle size and the support play a major role in the formation of coke during hydrocarbon reforming [42]. It is known that carbonaceous deposits appear on metal particles of larger size while lanthanum oxide promotes the adsorption of CO_2 forming lanthanum oxycarbonates ($La_2O_2CO_3$) which participate in coke gasification [22]. In agreement with this, the higher metal (Co + Ru) surface exposition observed for Ru-containing catalysts may contribute to the lower carbon concentration in these catalysts. Additionally to this reason, the lower carbon deposition may also be related to the presence of La in the catalysts. Some differences in the particle size of the $La_2O_2CO_3$ phase have found by XRD concentration on used catalysts (Fig. 9). Particle size of this

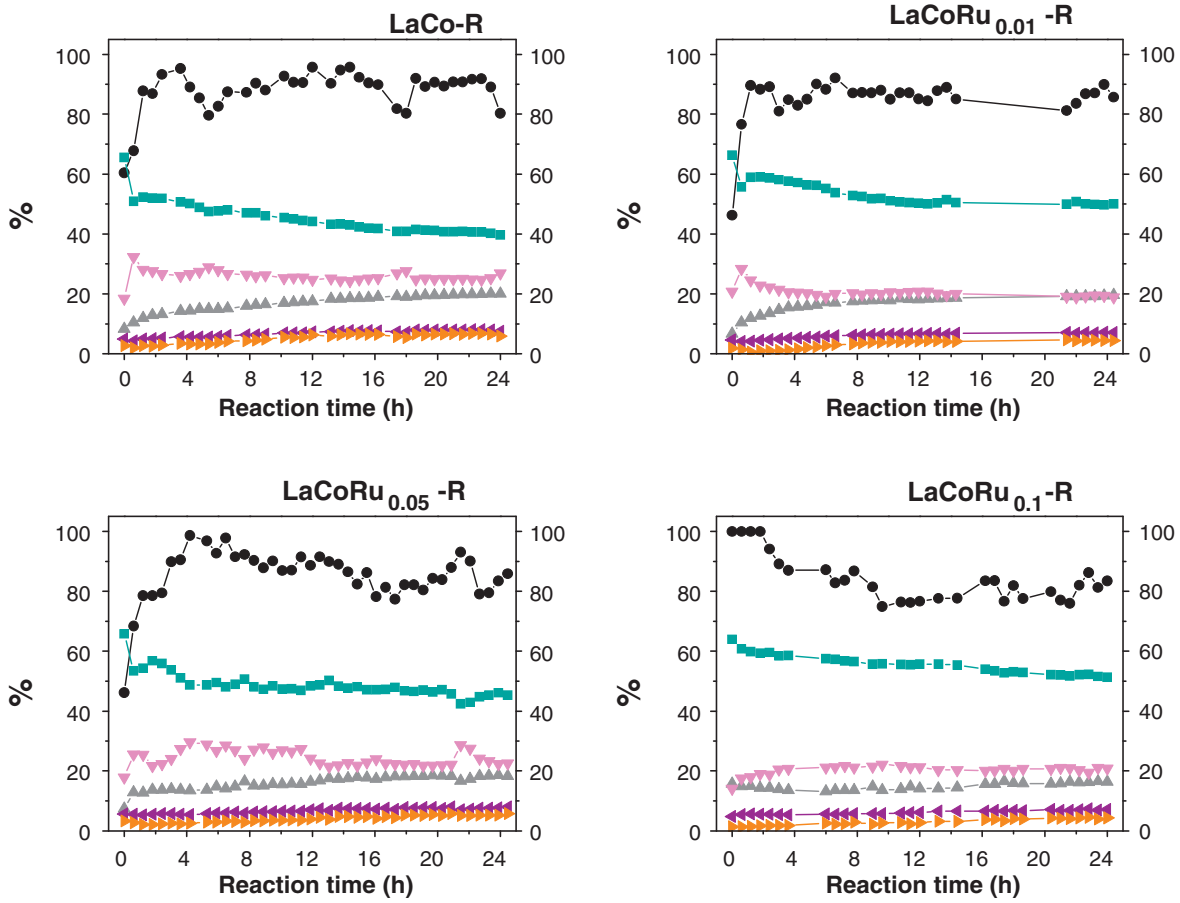

Fig. 8. Diesel conversion and product distribution during oxidative reforming of diesel over LaCo–R, $LaCoRu_{0.01}$–R, $LaCoRu_{0.05}$–R and $LaCoRu_{0.1}$–R catalysts ((–●–, %) diesel conversion, (–■–, %) H_2, (–▲–, %) CO, (–▼–, %) CO_2, (–◄–, %) CH_4, (–►–, %) C_2H_4, C_2H_6, C_3H_6, T = 1023 K, GHSV = 20,000 h^{-1}, 24 h, $H_2O/O_2/C$ = 3/0.5/1).

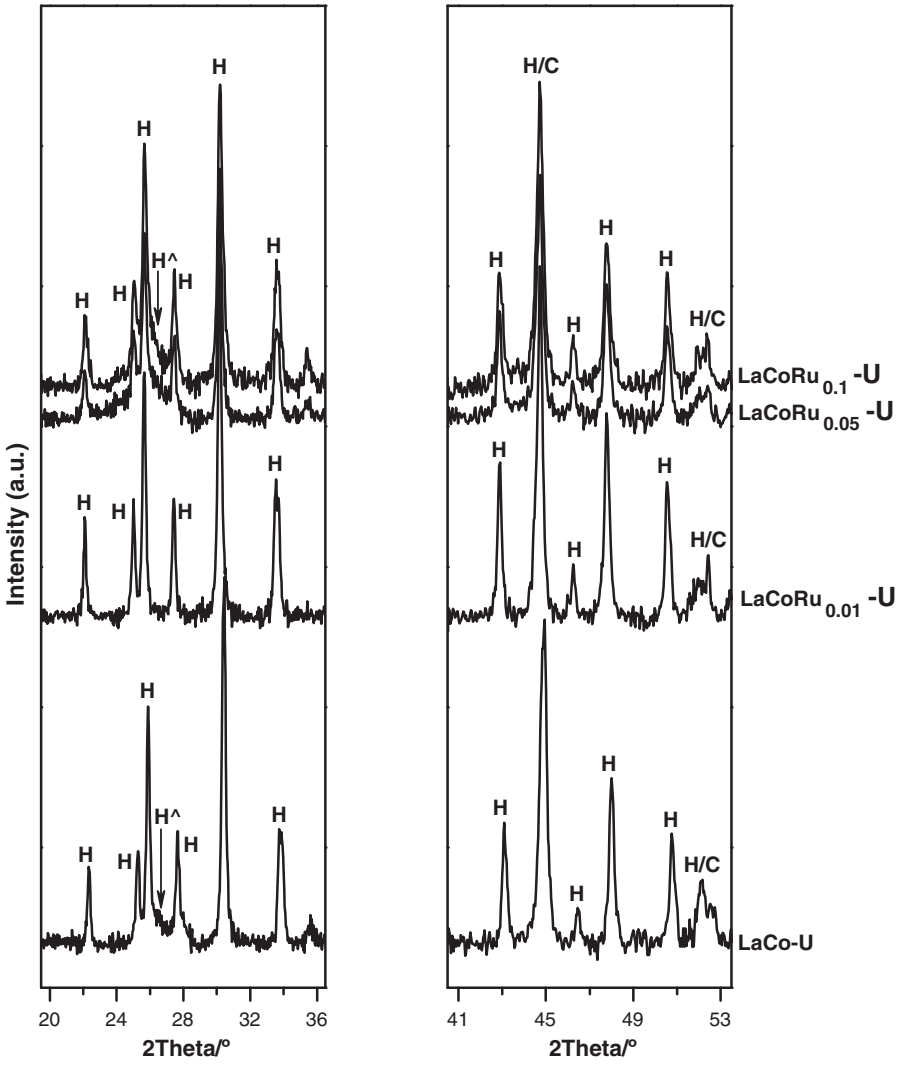

Fig. 9. XRD patterns of used catalysts (H: $La_2O_2CO_3$ hexagonal, C: Co^0 cubicand H: graphitic C).

$La_2O_2CO_3$ phase is lower in the more stable $LaCoRu_{0.1}$ catalyst. Therefore, it can be inferred some participation of lanthanum in the improvement in catalytic stability observed for the Ru-containing catalysts. From results presented here both effects, the higher active metal dispersion and the higher extension of the $La_2O_2CO_3$ phase, observed with the increase in the Ru substitution degree in the perovskites used as catalyst precursors may contribute to the enhancement in the reforming capacity and stability of the catalysts studied in this work.

5. Conclusions

The oxidative reforming of diesel over catalysts derived from $LaCo_{1-x}Ru_xO_3$ perovskites has been investigated with respect to the structural and morphological changes of catalysts derived from the substitution of Co by Ru ($x = 0.01$–0.1) in the perovskites. The substitution of cobalt by ruthenium in $LaCo_{1-x}Ru_xO_3$ perovskites modifies their physicochemical characteristics. It is observed that the increase in the Co substitution degree in the perovskite gradually changes the rhombohedral crystalline perovskite particles to orthorhombic particles of lower size. The modifications in the $LaCo_{1-x}Ru_xO_3$ perovskites directly affect its reduction behaviour and the structure and morphology of the derived catalysts formed after the thermal reduction. Better reducibility of the perovskite and better ruthenium and cobalt surface exposition and contact of metals with La_2O_3 after reduction were observed in catalysts derived from perovskites with higher degree of Co substitution by Ru. The catalytic activity strongly depends on characteristics of $LaCo_{1-x}Ru_xO_3$ perovskites used as precursors of catalysts, showing the catalyst derived from the perovskite with higher degree of Co substitution the higher activity and stability. The positive effect in reforming activity when ruthenium was included in the perovskite was inferred to be related with the higher active metal dispersion (Co + Ru) and the higher extension of the $La_2O_2CO_3$ phase observed in catalysts obtained after reduction of perovskites with higher Ru substitution degree.

Acknowledgements

We are grateful to our research sponsors, CAM (P2009/ENE-1743), INTA and King Saud University (Riyadh, Saudi Arabia). NMT would also like to acknowledge financial support from the JAE-CSIC grant programme and MCAG would also like to acknowledge financial support from the Ministry of Science and Innovation (Spain) through the R&C Programme.

References

[1] C.W. Forsberg, Prog. Nucl. Energy 51 (2009) 192.
[2] D. Chrenko, J. Coulié, S. Lecoq, M.C. Péra, D. Hissel, Int. J. Hydrogen Energy 34 (2009) 1324.
[3] J.D. Holladay, J. Hu, D.L. King, Y. Wang, Catal. Today 139 (2009) 244.
[4] A.F. Ghenciu, Curr. Opin. Solid State Mater. Sci. 6 (2002) 389.
[5] R.M. Navarro, M.A. Peña, J.L.G. Fierro, Chem. Rev. 107 (2007) 3952.
[6] D.K. Ross, Vacuum 80 (2006) 1084.
[7] U.K. Mirza, N. Ahmad, K. Harijan, T. Majeed, Renew. Sust. Energy Rev. 13 (2009) 1111.
[8] G. Babac, A. Sisman, T. Cimen, Int. J. Hydrogen Energy 34 (2009) 6357.
[9] S.L. Lakhapatri, M.A. Abraham, Appl. Catal. A: Gen. 364 (2009) 113.
[10] R. Kothari, D. Buddhi, R.L. Sawhney, Renew. Sust. Energy Rev. 12 (2008) 553.
[11] C. Horny, A. Renken, L. Kiwi-Minsker, Catal. Today 120 (2007) 45.
[12] A.M. Silva, A.M.D. Farias, d. Costa, L.O.O. Barandas, A.P.M.G. Mattos, L.V. Fraga, M.A.F.B. Noronha, Appl. Catal. A: Gen. 334 (2008) 179.
[13] A. Faur Ghenciu, Curr. Opin. Solid State Mater. Sci. 6 (2002) 389.
[14] M. Krumpelt, T.R. Krause, J.D. Carter, J.P. Kopasz, S. Ahmed, Catal. Today 77 (2002) 3.
[15] U.W. Carpenter, J.W. Hayes, CA 2325506 (1999).
[16] M. Ferrandon, T. Krause, Appl. Catal. A: Gen. 311 (2006) 135.
[17] E. Newson, T.B. Truong, Int. J. Hydrogen Energy 28 (2003) 1379.
[18] M. Krumpelt, T. Krause, J.D. Carter, J. Mawdsley, J.M. Bae, S. Ahmed, C. Rossignol, 2001 Annual DOE Report, Fuel Cells for Transportation, 2001.
[19] J.C. Amphlett, R.F. Mann, B.A. Peppley, P.R. Roberge, A. Rodrigues, J.P. Salvador, J. Power Sources 71 (1998) 179.
[20] R.M. Navarro, M.C. Álvarez-Galván, J.A. Villoria, I.D. González, F. Rosa, J.L.G. Fierro, Appl. Catal. B: Environ. 73 (2007) 247.
[21] N. Mota, M.C. Álvarez-Galván, J.A. Villoria, F. Rosa, J.L.G. Fierro, R.M. Navarro, Topics Catal. 52 (2009) 1995.
[22] J. Guo, H. Lou, Y. Zhu, X. Zhen, Mater. Lett. 57 (2003) 4450.
[23] P. Dinka, A.S. Mukasyan, J. Power Sources 167 (2007) 472.
[24] J.R. Mawdsley, T.R. Krause, Appl. Catal. A: Gen. 334 (2008) 311.
[25] G.C.d. Araujo, S.M.d. Lima, J.M. Assaff, M.A. Peña, J.L.G. Fierro, M. do Carmo Rangel, Catal. Today 133–135 (2008) 129.
[26] N.H. Batis, P. Delichere, H. Batis, Appl. Catal. A: Gen. 282 (2005) 173.
[27] M.P. Pechini, United States Patent Office 3,330,673 (1967).
[28] C.D. Wagner, L.E. Davis, M.V. Zeller, J.A. Taylor, R.H. Raymond, L.H. Gale, Surf. Interf. Anal. 3 (1981) 211.
[29] S. Ivanova, A. Senyshyn, E. Zhecheva, K. Thenchev, R. Stoyanova, H. Fuess, J. Solid State Chem 183 (4) (2010) 940–950.
[30] N. Ramadass, Mater. Sci. Eng. 36 (1978) 231.
[31] J. Dullac, Bull. Soc. Fr. Miner. Crystallogr. 92 (1969) 487.
[32] E. Iglesia, S.L. Soled, R.A. Fiato, G.H. Via, J. Catal. 143 (1993) 345.
[33] V. Szabo, M. Bassir, A. van Neste, S. Kaliaguine, Appl. Catal. B 37 (2002) 175.
[34] L. Huang, M. Bassir, S. Kaliaguine, Appl. Surf. Sci. 243 (2005) 360.
[35] E.A. Lombardo, K. Tanaka, I. Toyoshima, J. Catal. 80 (1983) 340.
[36] L. González Tejuca, A.T. Bell, J.L.G. Fierro, M.A. Peña, Appl. Surface Sci. 31 (1988) 301.
[37] Y. Zhu, R. Tan, J. Feng, S. Ji, L. Cao, Appl. Catal. A: Gen. 209 (2001) 71.
[38] L. Armelao, G. Bandoli, D. Barreca, M. Bettinelli, G. Bottaro, A. Caneschi, Surf. Interface Anal. 34 (2002) 112.
[39] J.M. Giraudon, A. Elhachimi, F. Wyrwalski, S. Siffert, A. Aboukaïs, J.F. Lamonier, G. Leclercq, Appl. Catal. B: Environ. 75 (2007) 157.
[40] J.M. Giraudon, A. Elhachimi, G. Leclercq, Appl. Catal. B: Environ. 84 (2008) 251.
[41] M.A. Peña, J.L.G. Fierro, Chem. Rev. 101 (2001) 1981.
[42] J.R. Rostrup-Nielsen, in: J.R. Anderson, M. Boudart (Eds.), Catalysis, Science and Technology, vol. 5, Springer-Verlag, Berlin, 1984.